ISSUE: March 2024

How Active EMI Filter ICs Reduce Common-Mode Emissions In Single- And Three-Phase Applications (Part 3): Modeling Nanocrystalline Chokes

by Timothy Hegarty, Texas Instruments, Phoenix, Ariz.

A compact and efficient design of the electromagnetic interference (EMI) filter is, increasingly, one of the main challenges in a high-density switching regulator. Multistage passive filters provide high rolloff and are common in high-power ac line applications where common-mode (CM) asymmetrical interference currents are more difficult to manage than differential-mode (DM) currents.

Part 1 of this article series[1] provided an overview of active EMI filter (AEF) techniques to diminish the reliance on bulky passive filter components. An AEF circuit can significantly reduce magnetic component and overall filter size vis-à-vis an equivalent passive filter, enabling higher-density filter designs for size-constrained applications. Part 2 discussed impedance characterization for a ferrite choke[2] over a required frequency range using a behavioral model, which is an essential step and of paramount importance in EMI filter design, as the choke impedance directly impacts filter attenuation performance (as well as loop stability in active designs).

More challenging to model than ferrite, however, is a choke with nanocrystalline core material,[3-11] given its frequency-dependent and nonlinear magnetic permeability. It is for this reason that this article examines comprehensive simulation models for nanocrystalline-cored chokes, with the objective to design and use these magnetic components in both passive and active[12] filter circuits.

Following a review of complex permeability and its impact on the impedance behavior of ferrite and nanocrystalline chokes, this article describes a SPICE-compatible behavioral model for a nanocrystalline CM choke using an intuitive ladder circuit structure. This model facilitates easy and accurate system-level simulation in the time and frequency domains for both passive and active filter designs.

Using an extraction procedure of model parameters from measured impedance data, the synthetized behavioral model for the choke impedance can accommodate single- and three-phase chokes. The article concludes with a practical example, applying a modeling procedure to a three-phase four-winding nanocrystalline choke used in an EMI filter for an automotive onboard charger (OBC) application.

Impedance Behavior Of Ferrite And Nanocrystalline Chokes

Increasingly used in high-current EMI filter designs, a choke with nanocrystalline core material combines high magnetic permeability (μ_i, approximately 10,000 to 200,000), high saturation induction (B_{SAT}, approximately 1.2 T), a high permissible operating temperature ($T_{OP\text{-}MAX}$ > 120°C), and stable magnetic properties over a wide temperature range.[4-7] A typical composition of nanocrystalline alloy is $Fe_{73.5}Cu_1Nb_3Si_{15.5}B_7$. Common trade names for nanocrystalline include Vitroperm from Vacuumschmelze,[5, 6] Finemet from Hitachi Metals and Nanoperm from Magnetec.

Despite a cost increment relative to their ferrite counterparts, nanocrystalline chokes deliver a high-performance alternative for EMI filter circuits. Typically offered in toroidal shapes, because of its material brittleness a nanocrystalline core is epoxy-coated or placed in a plastic enclosure.

Fig. 1 compares the typical impedance magnitude and phase profiles versus frequency for ferrite and nanocrystalline CM choke samples. At the crucial lower frequency boundary for EMI measurement of 150 kHz, the chokes as selected each have an impedance of approximately 320 Ω, corresponding to a nominal inductance of 340 µH. This is a fair approach when the necessary impedance at 150 kHz usually defines the CM choke in practical filter applications. In other words, the lowest frequency effectively sets the required inductance of the CM choke.

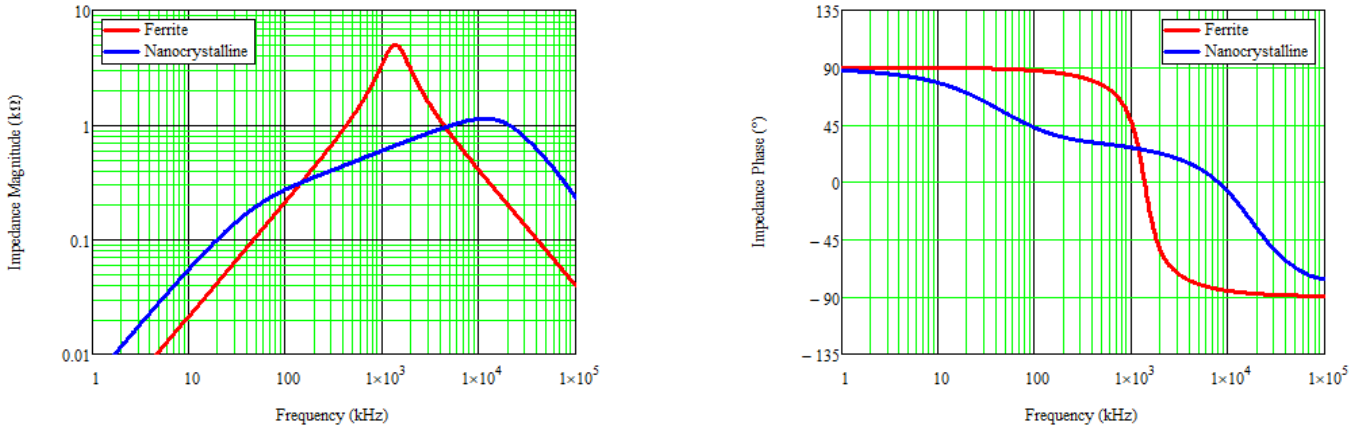

Fig. 1. Typical impedance magnitude (a) and phase (b) characteristics vs. frequency for chokes with ferrite and nanocrystalline core materials. The impedances are set equal at 150 kHz for objective comparison.

With higher initial permeability and a lower winding capacitance, nanocrystalline chokes provide broadband suppression with better attenuation relative to ferrite at both low and high frequencies. However, as shown in Fig. 1, ferrite often provides higher impedance in the critical mid-frequency range, albeit at the expense of a larger overall component size. To achieve similar inductance at 150 kHz and a dc winding resistance comparable to a nanocrystalline choke, a ferrite core typically has a 30% larger form factor to accommodate more winding turns with heavier-gauge wire.[10]

As described in part 2 of this article series[2] and illustrated in Fig. 1a above, the asymptotes of the impedance magnitude characteristic for a ferrite occur at |20dB| per decade on either side of the self-resonant peak, and the phase displays a high-Q transition from 90°to –90°. In contrast, while the nanocrystalline choke impedance increases at 20 dB per decade at low frequencies, a shallower impedance slope is evident above approximately 40 kHz in this example. Also, the phase of the impedance starts at 90°but gradually decreases to 0° around the impedance peak, softly converging thereafter toward –90°as the impedance becomes capacitive-dominant. As expected, a phase of ±45°indicates an equal balance of resistive and reactive impedances.

As detailed in the next section, the change of upslope in the nanocrystalline impedance curve of Fig. 1a relates to the reactive component of impedance rolling off and the corresponding increase of the resistive component. The associated softer-phase behavior results in a lower Q and a damped EMI filter characteristic behavior.

Complex Magnetic Permeability

The complex permeability characteristic is an essential quantity to characterize magnetic performance, especially for EMI applications, as it defines the choke impedance behavior in the frequency domain. The series model for the complex permeability of a core is expressed by its real (inductive) component μ_s' and imaginary (dissipative) component μ_s''. An equivalent circuit in which an equivalent loss-free inductance $L_s(\omega)$ connects in series with an equivalent loss resistance $R_s(\omega)$ can then represent a choke with *N* turns.

Equation 1 describes the choke impedance vector as:

$$Z_L(\omega) = j\omega L_s(\omega) + R_s(\omega) \equiv j\omega L_0\left[\mu_s'(\omega) - j\mu_s''(\omega)\right] \qquad (1)$$

$$L_0 = \frac{\mu_0 N^2 A_c}{l_c}; \quad \tan\delta_m(\omega) = \frac{\mu_s''(\omega)}{\mu_s'(\omega)}$$

where ω is the angular frequency, *j* is the complex operator, L_0 is the inductance at unity relative permeability, A_c is the core effective cross-sectional area, l_c is the magnetic flux mean path length, and the permeability of free space is $\mu_0 = 4\pi \times 10^{-7}$ H/m. The tangent of the loss angle $\delta_m(\omega)$ describes the power losses.

The frequency dependences of the real and imaginary parts of complex permeability represent significant core material properties and are typically listed in the data sheet for a particular core material. At low frequencies, the permeability is a real number as the vectors of flux density *B* and field intensity *H* are in phase. However, the phase shift between the *B* and *H* vectors increases at high frequency, caused by eddy currents and magnetic losses in the core material.

An alternative formulation considers the effective complex relative permeability μ_r of the overall magnetic design, consisting of $\mu_r'(\omega)$ and $\mu_r''(\omega)$ as its real and imaginary parts, where equations 2 and 3 give expressions for the impedance and loss tangent:

$$\begin{aligned} Z_L(\omega) &= j\omega\mu_0\mu_r(\omega)\frac{N^2A_c}{l_c} \\ &= j\omega\left[\mu_r'(\omega) - j\mu_r''(\omega)\right]\frac{\mu_0N^2A_c}{l_c} \end{aligned} \qquad (2)$$

$$\left|\mu_r(\omega)\right| = \sqrt{\mu_r'(\omega)^2 + \mu_r''(\omega)^2}, \quad \tan\delta_\mu(\omega) = \frac{\mu_r''(\omega)}{\mu_r'(\omega)} \qquad (3)$$

The effective complex permeability model represents the physical behavior of a real choke. Equating the real and imaginary parts of equations 1 and 2, equation 4 represents each part of the effective complex permeability in terms of a frequency-dependent series resistance and inductance as:

$$\begin{aligned} \mu_r'(\omega) &= \frac{l_c}{\mu_0N^2A_c}\cdot\frac{X_s(\omega)}{\omega} = \frac{l_c}{\mu_0N^2A_c}\cdot L_s(\omega) \\ \mu_r''(\omega) &= \frac{l_c}{\mu_0N^2A_c}\cdot\frac{R_s(\omega)}{\omega} \end{aligned} \qquad (4)$$

More practically, equation 5 derives the effective real and imaginary permeabilities if the choke impedance magnitude and phase data vs. frequency can be measured directly using a vector network analyzer (VNA) or impedance analyzer (IA).

$$\begin{bmatrix}\mu_r'(f)\\ \mu_r''(f)\end{bmatrix} = \frac{l_c}{2\pi f\mu_0N^2A_c}\cdot\begin{bmatrix}\mathrm{Im}\{Z_L(f)\}\\ \mathrm{Re}\{Z_L(f)\}\end{bmatrix} = \frac{l_c}{2\pi f\mu_0N^2A_c}\cdot\left|Z_L(f)\right|\cdot\begin{bmatrix}\sin\theta(f)\\ \cos\theta(f)\end{bmatrix} \qquad (5)$$

Of course, the effective or apparent complex permeability characteristics depend on the core geometry and winding structure and thus are unique for each choke setup. In contrast, the intrinsic permeability data given by core manufacturers applies only to close-to-ideal magnetic components and is valid away from self-resonance.

If the geometric configuration of a toroidal ring core is represented by its height h_c, inner radius r_i and outer radius r_o, then equation 6 expresses the real and imaginary permeabilities as:

$$\begin{bmatrix}\mu_r'(f)\\ \mu_r''(f)\end{bmatrix} = \frac{\left|Z_L(f)\right|}{h_c ln\left(\frac{r_o}{r_i}\right)f\mu_0N^2}\cdot\begin{bmatrix}\sin\theta(f)\\ \cos\theta(f)\end{bmatrix} \qquad (6)$$

Fig. 2 illustrates the complex permeability behavior over frequency based on the impedance curves for the ferrite and nanocrystalline chokes given in Fig. 1. The imaginary part of complex permeability reaches at maximum at a characteristic resonant frequency. Below this frequency, the real component of complex permeability remains close to the initial permeability, while the imaginary component progressively increases until it reaches its maximum value. This phenomenon is due to magnetic losses within the core that increase the impedance. Above the resonant frequency, the behavior of the core changes as both the real and imaginary components of permeability decrease.

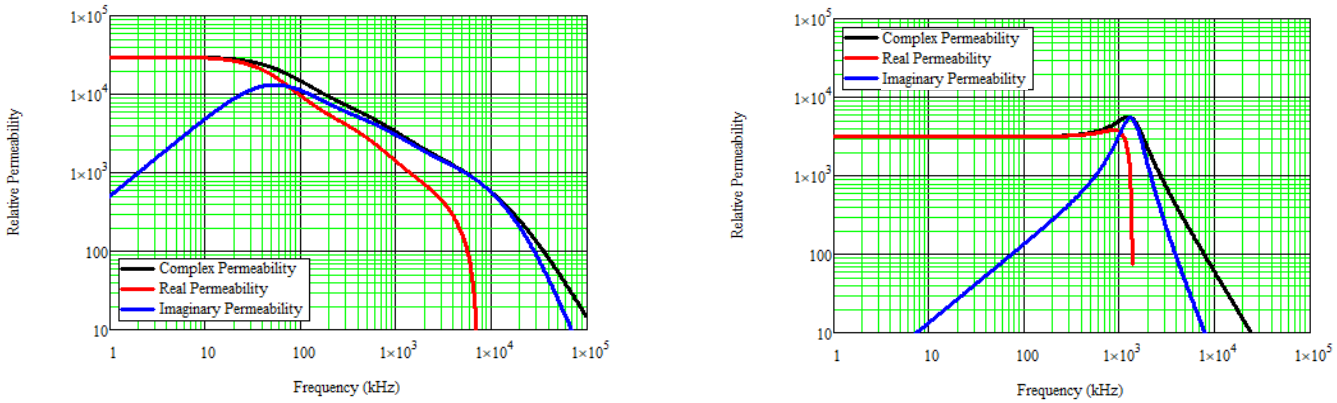

Fig. 2. Effective complex relative permeability plots for chokes with nanocrystalline (a) and ferrite (b) core material.

As indicated in Fig. 2, the nanocrystalline material has much higher initial permeability than the ferrite, 30,000 vs. 3,000, and thus requires fewer winding turns for a given inductance (typically specified at 10 kHz). However, the permeability of the nanocrystalline rolls off at a lower frequency than the ferrite, as expected. Fig. 3 shows the variation of effective series resistance and inductance for the nanocrystalline and ferrite chokes.

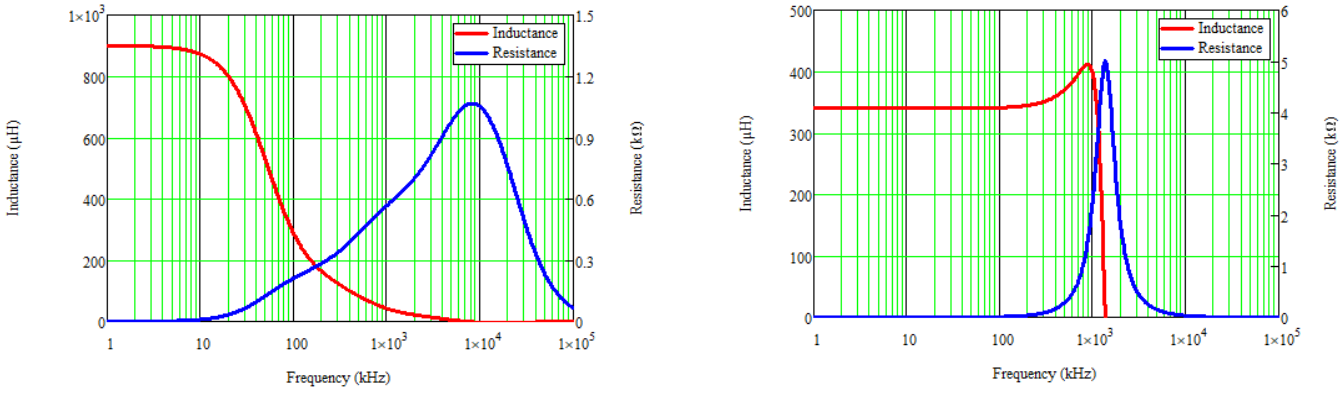

Fig. 3. Effective inductance and resistance versus frequency for nanocrystalline (a) and ferrite (b) chokes.

Clearly, the nanocrystalline core exhibits an earlier rolloff of inductance with frequency than a ferrite, but the net choke impedance is buoyed by its inherently higher resistance contribution. The peak of resistance in Fig. 3a aligns with the resonant frequency from Fig. 1a. Higher attenuation and an extended operating temperature range enable a reduction of the component volume vis-à-vis ferrite under similar conditions.[10] However, as outlined in the next section, the nonlinear impedance characteristic of nanocrystalline requires a different

behavioral model than ferrite. See part 2 of this article series[2] for a detailed discussion on modeling ferrite chokes.

Behavioral Model For A Nanocrystalline Choke

Circuit simulation is essential for the effective design of EMI filters, but accurate simulation requires precise circuit models of filter components, especially the CM choke. Because construction data and other basic parameters such as properties of the core material are not always available from magnetic vendors or respective data sheets to create a physical model, let's instead focus on a behavioral model for a choke based on the measured small-signal impedance (magnitude and phase data).

Fig. 4 shows a proposed behavioral model[11] for a nanocrystalline choke consisting of a ladder network with concatenated RL-parallel circuits, also known as a Foster-type series network, in parallel with the parasitic intrawinding capacitance, C_W.

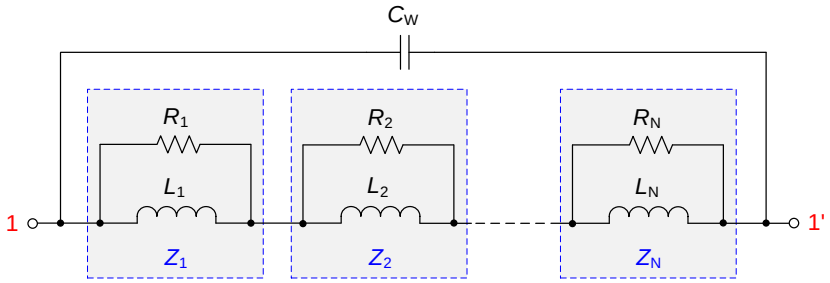

Fig. 4. Proposed behavioral model consisting of cascaded RL circuits to model the impedance of a nanocrystalline choke.

This behavioral model easily implements in any circuit simulator and is suitable for both time- and frequency-domain simulations (especially since the model uses no Laplace elements). As expected, the approximation accuracy improves with an increasing number of RL-parallel circuits. However, the computational complexity increases as well, requiring the optimization of more parameters.

Practical experience with nanocrystalline CM chokes reveals that three or four RL circuits in series are generally adequate for a sufficiently accurate fit of the impedance magnitude and phase characteristics. Equation 7 expresses the total impedance of the model in Fig. 4.

$$Z_L(s) = \left[Z_{foster}(s)^{-1} + sC_W \right]^{-1} = \left[\left(\sum_{i=1}^{N} \left(\frac{1}{R_i} + \frac{1}{sL_i} \right)^{-1} \right)^{-1} + sC_W \right]^{-1} \quad (7)$$

As shown in Fig. 5, the proposed model derives as an RL ladder network from a single RL-parallel circuit by repeated manipulation called circuit dividing,[11] which is a term referring to the transformation of a single RL-parallel circuit into two series-connected RL-parallel circuits, thus improving the accuracy of the shaped impedance result relative to the target impedance characteristic.

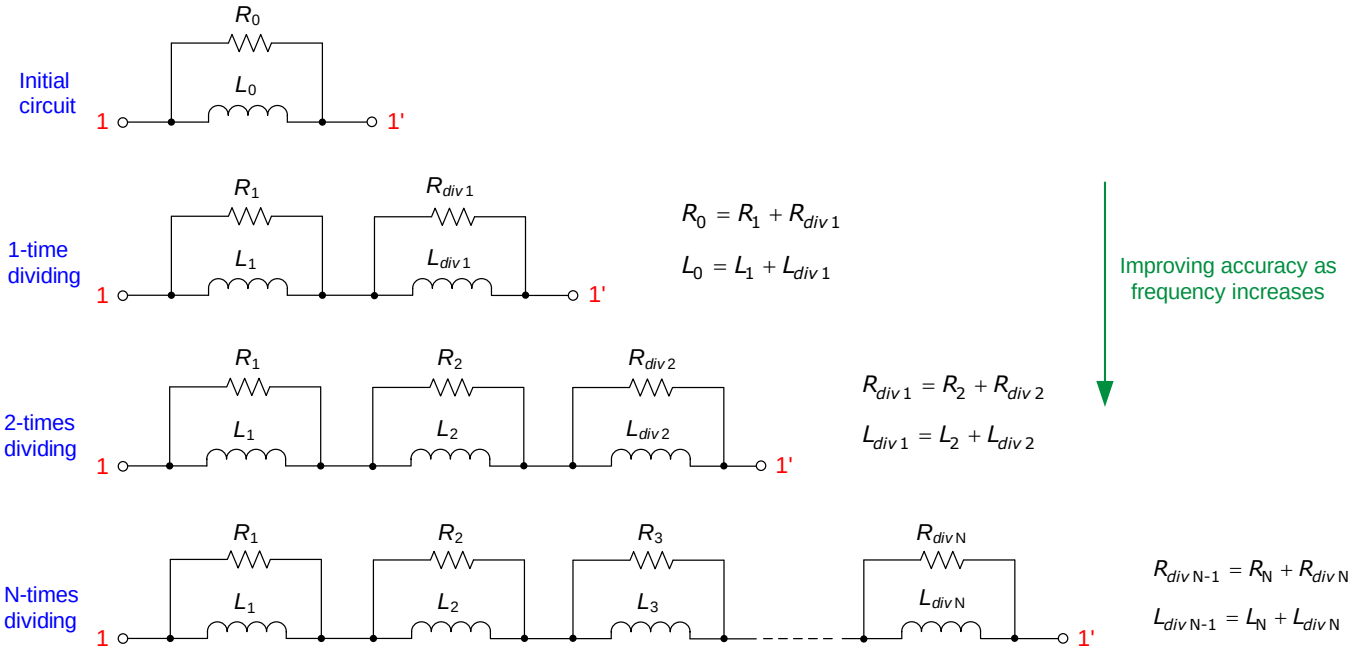

Fig. 5. Model development by repeated RL circuit divisions, each of which improves fitting accuracy as the frequency increases.

Only two parameters, denoted as R_N and L_N, need fitting at each step. The accuracy of the approximation progressively improves from low to high frequencies with each circuit division. Equation 8 offers generalized expressions for circuit dividing:

$$\begin{aligned} R_{i-1} &= R_i + R_{div\,i} \quad \text{with } R_i \le R_{div\,i} \\ L_{i-1} &= L_i + L_{div\,i} \quad \text{with } L_i \ge L_{div\,i} \end{aligned} \qquad i \ge 1 \qquad (8)$$

where R_i and L_i are the two fitted parameters.

Each successive RL circuit has lower inductance and higher resistance than its preceding counterpart, thus suitably shaping the impedance profile to that of a nanocrystalline choke as the frequency increases.

More formally, equation 9 optimizes resistances R_i, $R_{div\,i}$ and inductances L_i, $L_{div\,i}$ by adjusting two parameters, a_i and b_i:

$$\begin{aligned} R_i &= \frac{R_{div\,i-1}}{2}(1-a_i), \quad R_{div\,i} = \frac{R_{div\,i-1}}{2}(1+a_i), \quad 0 \le a_i \le 1 \ \ (i = 1,2,\ldots,N) \\ L_i &= \frac{L_{div\,i-1}}{2}(1+b_i), \quad L_{div\,i} = \frac{L_{div\,i-1}}{2}(1-b_i), \quad 0 \le b_i \le 1 \ \ (i = 1,2,\ldots,N) \end{aligned} \qquad (9)$$

Sum $a_i + b_i$ determines the magnitude reduction at the corner frequency of the original LR circuit, and b_i then controls the phase for a constant value of $a_i + b_i$. An analytical approach[11] makes use of these two findings. However, the hand method discussed in the next section is generally sufficient.

Fig. 6 illustrates the impedance of individual RL circuits and how they each contribute to the total impedance. Fig. 6b, for instance, shows how the individual impedance profiles, denoted as Z_1, Z_2 and Z_3, of three series RL circuits, serve to shape the low-, mid- and high-frequency profiles, respectively, of the overall impedance characteristic (denoted in blue).

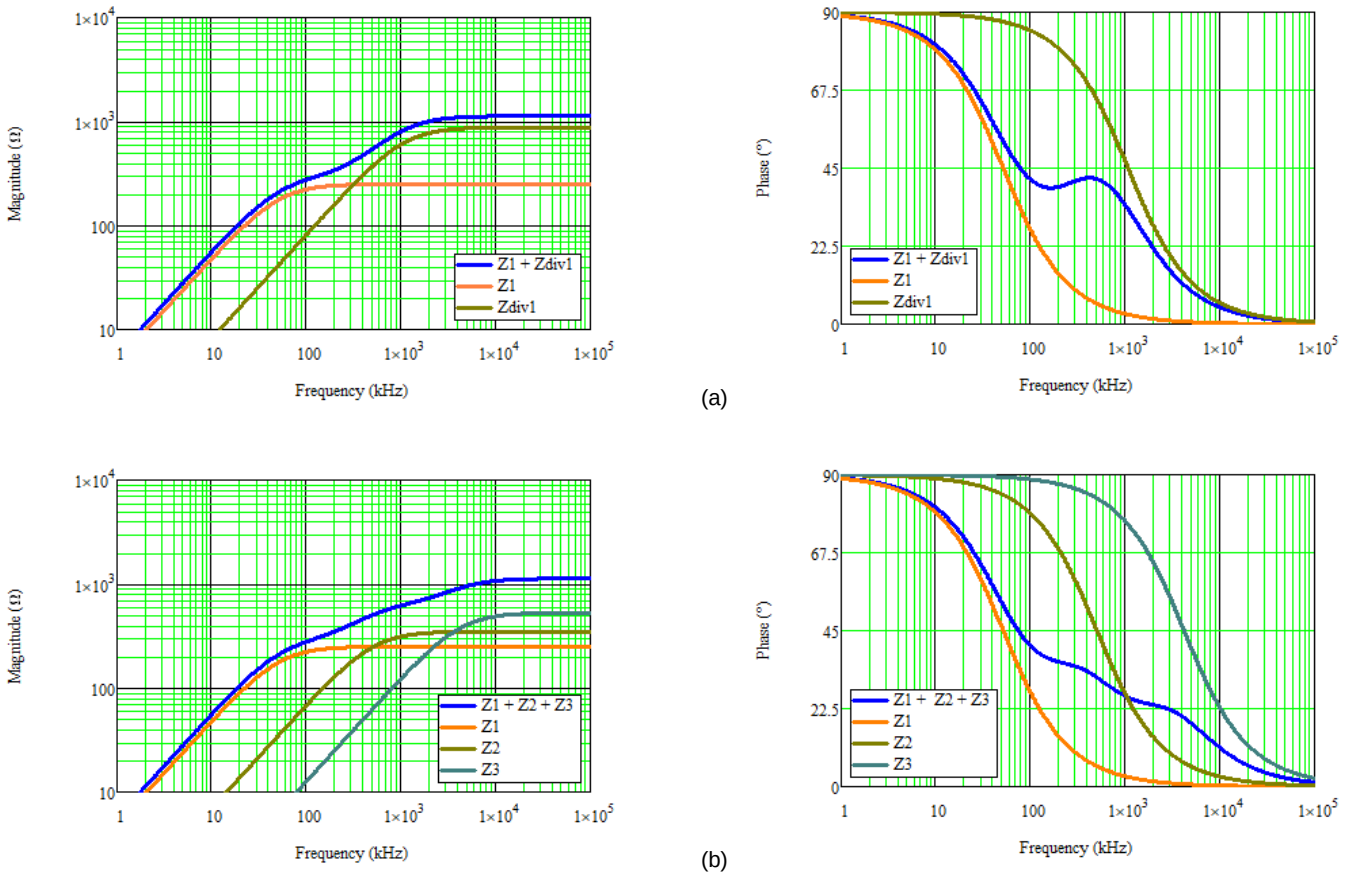

Fig. 6. Impedance shaping arising from circuit dividing using a cascaded connection of two (a) and three (b) RL-parallel circuits.

Applying the procedure for impedance scaling[2] for multiple windings to the basic choke model shown in Fig. 7a and using ideal coupled inductors with a mutual coupling factor k = 1, the schematics of Fig. 7 parts b and c typify practical model realizations for single-phase (two-winding) and three-phase (four-winding) CM chokes.

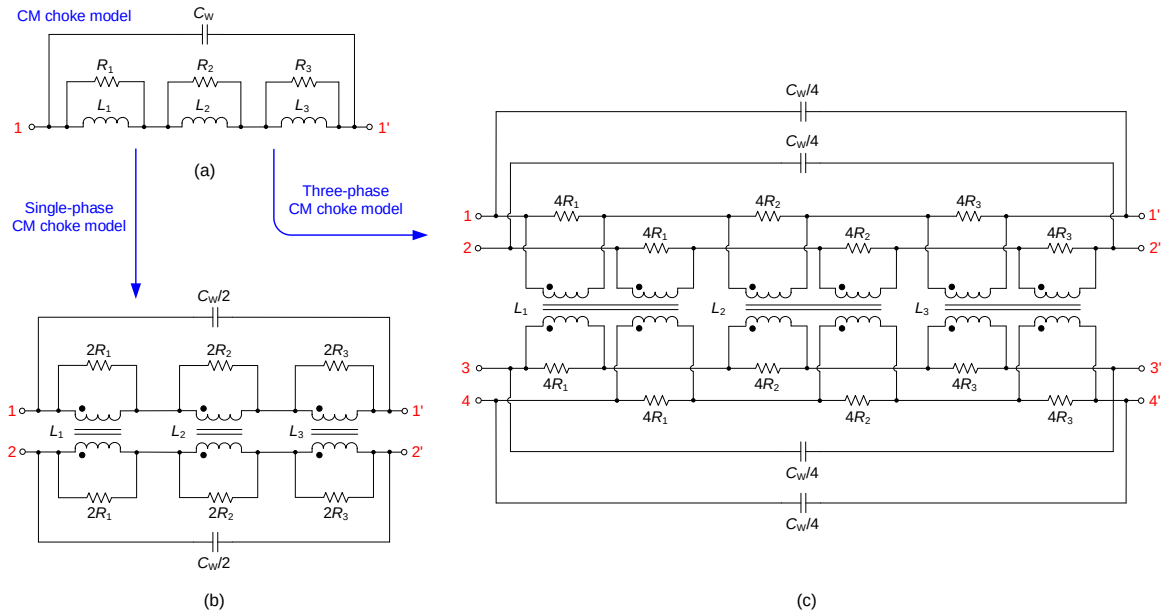

Fig. 7. Behavioral model for a nanocrystalline CM choke using three cascaded RL-parallel circuits (a) translated by impedance scaling into practical realizations for the simulation of single-phase (b) and three-phase (c) chokes.

Not shown in Fig. 7 parts b and c, but easily included if needed, are elements for dc winding resistance, leakage inductance and interwinding capacitance. Review the ferrite choke models presented in part 2[2] for a template to incorporate these additional elements if needed.

Parameter Extraction Example

A CM choke with nanocrystalline core serves as a test case to prove the effectiveness of the proposed method both in terms of accuracy and ease of implementation. Fig. 8 shows a three-phase EMI filter implementation using the TPSF12C3 AEF device[12] from Texas Instruments. The filter is a two-stage design using two nanocrystalline CM chokes (Würth Elektronik 7448340107480). Fig. 9 shows the development flow of the model for this choke, beginning with the initial RL circuit fitting and progressing to a final three-phase model realization.

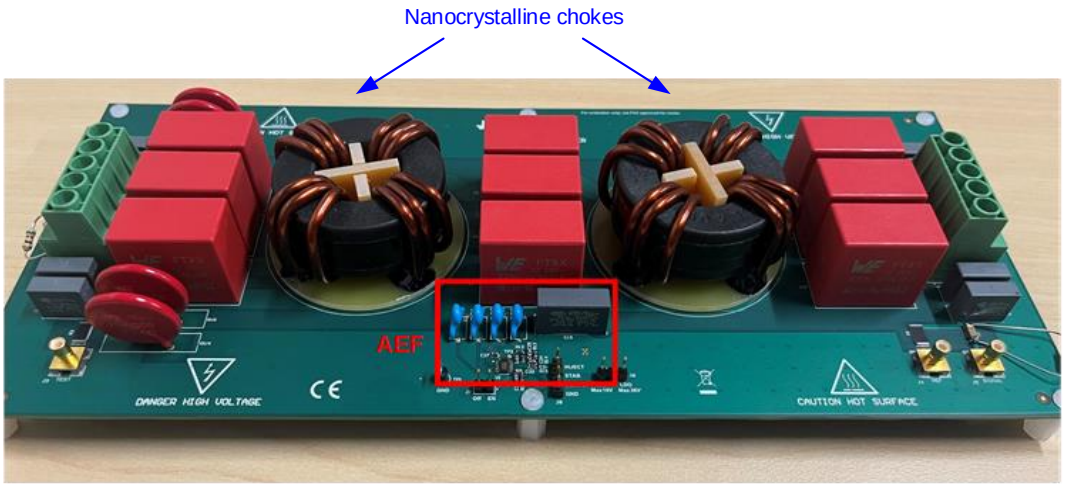

Fig. 8. Three-phase EMI filter design with AEF rated at 32 Arms per phase for a 22-kW OBC. The CM choke inductance specification is 0.75 mH at 10 kHz.

The impedance magnitude and phase curves as presented in red in Fig. 10 represent the measured choke impedance data (using a VNA or IA), enabling a direct comparison to each iteration of the model as it develops. Two circuit divisions expand the region of high accuracy as the frequency increases.

Let's summarize the procedure to fit to the measured impedance profile by circuit dividing:

1. First, determine the frequency region of interest—from 1 kHz to the impedance peak at 10 MHz—and conduct a fitting with a single RL-parallel circuit, as denoted by R_0 and L_0 in Fig. 5. As shown in Fig. 9a, set the inductance to 900 µH to match the low-frequency impedance and adjust the resistance to 1.13 kΩ to correspond to the maximum impedance amplitude within the frequency range of interest. According to Fig. 10a, the fitted result developed as a starting point is accurate at low frequencies but shows a sizeable error in both amplitude and phase at medium and high frequencies.

2. Next, conduct circuit dividing to improve the fitting precision, either by hand or analytically.[12] As it is difficult to fit over the whole frequency region with just one circuit division, consider just the mid-frequency range, roughly 20 kHz to 100 kHz. Divide the [900 µH, 1.3 kΩ] RL circuit from step 1 and iterate to a fit using [770 µH, 250 Ω] and [130 µH, 880 Ω], as shown in Fig. 9b. According to Fig. 10b, circuit dividing improves the fitting accuracy in the low-frequency region, but an error still remains at high frequencies.

3. Repeat the circuit dividing, thus improving the fitting accuracy at high frequency while retaining the already high precision in the low- and mid-frequency regions. Divide the [130 µH, 880 Ω] RL circuit from step 2 into [110 µH, 350 Ω] and [20 µH, 530 Ω], as shown in Fig. 9b. The model now matches the measured data reasonably well for both magnitude and phase up to 10 MHz. Further circuit dividing is not required.

4. Finally, add a parasitic capacitance of 5.6 pF as shown in Fig. 9d to fit the high-frequency rolloff of the impedance magnitude above 10 MHz. From that, you can generate the three-phase circuit realization by simple impedance scaling of the resistive and capacitive component values according to the number of power lines. This choke model is now ready for inclusion in a system-level EMI filter simulation schematic.[1]

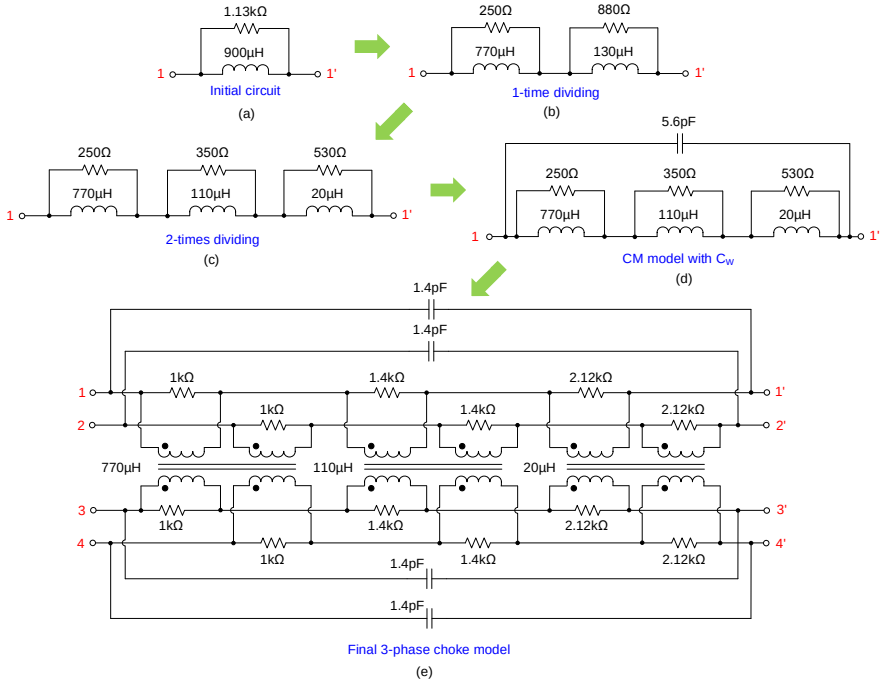

Fig. 9. Example of the model development flow for a three-phase CM choke.

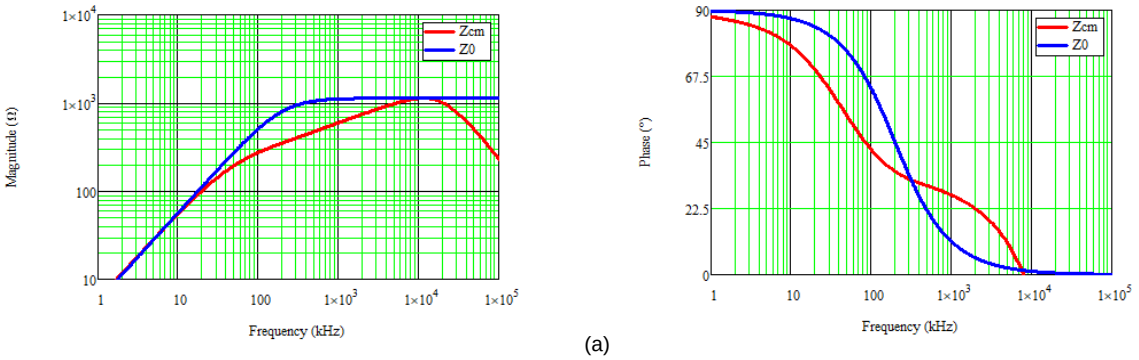

(a)

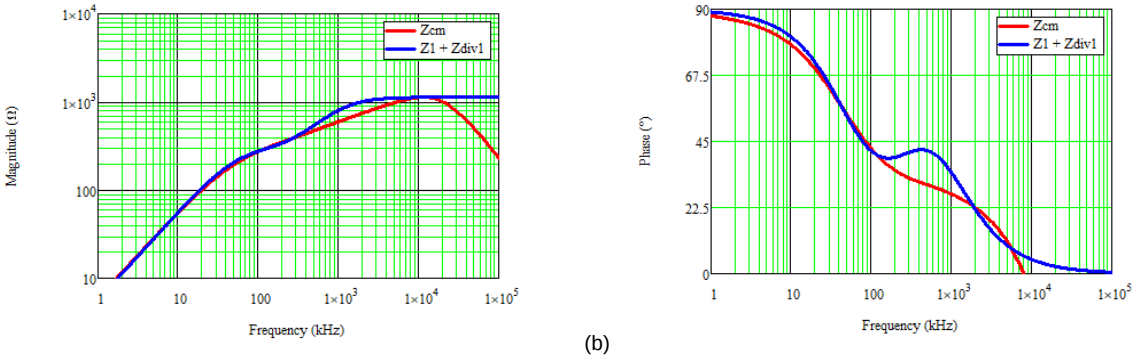

(b)

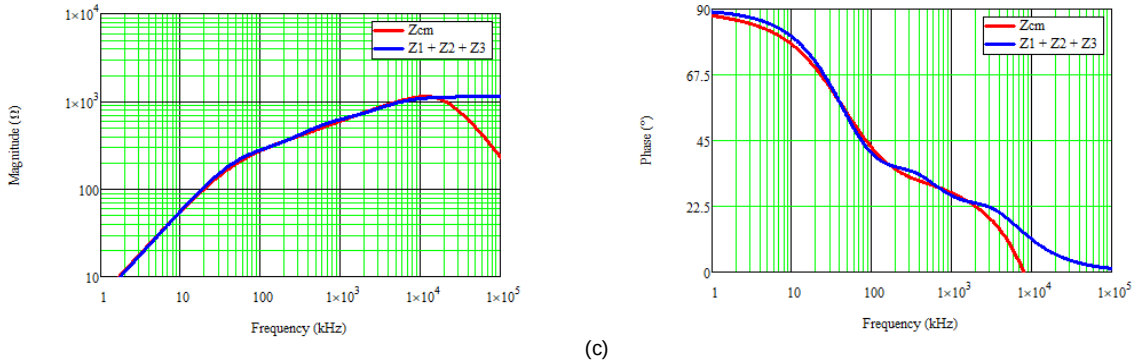

(c)

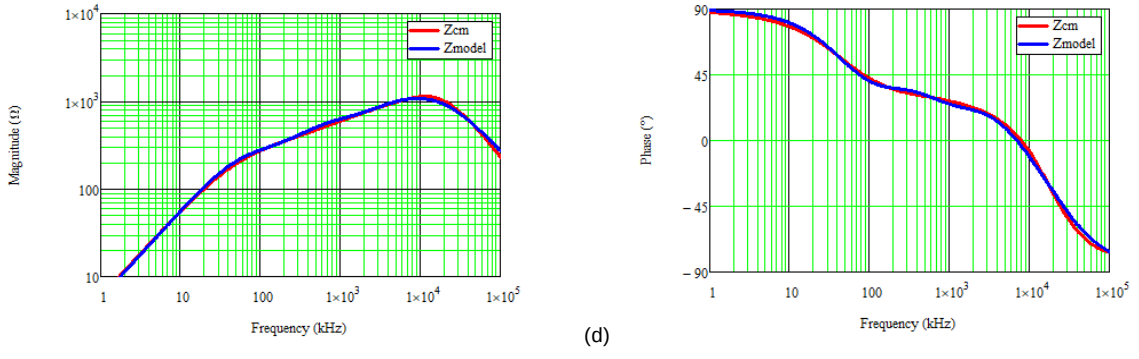

(d)

Fig. 10, Impedance characteristics of the circuits from Fig. 9 with one (a), two (b) and three (c) RL-parallel circuits, and the final model including parasitic winding capacitance (d).

Summary

In terms of damping effect, power losses, temperature stability, size and weight requirements, range of frequency, rated current, and rated inductance, it's easy to see why nanocrystalline chokes are popular in high-current EMI filters, especially since the CM chokes are often the largest components in the whole design. From this standpoint, having accurate, easy-to-use choke models for system-level EMI simulation in the time and frequency domains is an important requirement in the design of EMI filter circuits.

This article highlights the derivation of a choke model for nanocrystalline chokes that have a nonlinear permeability characteristic with frequency, synthesizing the measured impedance curve into a suitable RL-ladder Foster network that is physically intuitive and easy to parameterize. It is possible to implement such behavioral models in any circuit sim4ulator. Using a CM choke with a nanocrystalline core as a test case proves the effectiveness of the proposed method in terms of both accuracy and ease of implementation.

References

1. "How Active EMI Filter ICs Reduce Common-Mode Emissions In Single- And Three-Phase Applications (Part 1): An Overview" by Timothy Hegarty, How2Power Today, November 2023 Issue.
2. "How Active EMI Filter ICs Reduce Common-Mode Emissions in Single- And Three-Phase Applications (Part 2): Modeling Ferrite Chokes" by Timothy Hegarty, How2Power Today, February 2024 Issue.
3. "Magnetic material selection for EMI filters" by Marcin Kacki, Marek S. Rylko, John G. Hayes and Charles R. Sullivan, 2017 IEEE Energy Conversion Congress and Exposition (ECCE), October 2017, pp. 2350-2356.
4. "EMC Products Based on Nanocrystalline Vitroperm." Vacuumschmelze, 2021.
5. "Actual and Future Developments of Nanocrystalline Magnetic Materials for Common Mode Chokes and Transformers," by Holger Schwenk, Johannes Beichler, Werner Loges and Christian Scharwitz, PCIM Europe, May 2015, pp. 209-216.
6. "Nanocrystalline Soft Magnetic Metal Core Materials Explained," Passive Components blog, Dec. 18, 2020.
7. "Soft Magnetic Materials for a Sustainable and Electrified World" by Josefina M. Silveyra, Enzo Ferrara, Dale L. Huber and Todd C. Monson. Published in Science, 362, No. 6413, October 26, 2018.
8. "Comparison of High-Frequency Ferrite and Nanocrystalline Core Losses Using Identical Geometries" by Roderick A. Gomez, David A. Porras Fernandez, German G. Oggier, Juan C. Balda and Yue Zhao. Published in 2022 IEEE 13th International Symposium on Power Electronics for Distributed Generation Systems (PEDG), Kiel, Germany, June 2022, pp. 1-5.
9. "Nanocrystalline magnetic materials versus ferrites in power electronics" by Georgi T. Nikolov and Vencislav C. Valchev. Sixth International Conference on Mining Science & Technology (ICMST) 1, No. 1 (September 2009): pp. 1357-1361.
10. "Nanocrystalline Replaces High Perm Ferrite in Common Mode Chokes" by Rob Flaherty. MH & W International Corp., August 8, 2017.
11. "Straightforward Modeling of Complex Permeability for Common Mode Chokes" by Katsuya Nomura, Takashi Kojima and Yoshiyuki Hattori. Published in IEEJ Industry Applications 7, No. 6 (November 2018): pp. 462-472.
12. "TPSF12C1 and TPSF12C3 power-supply filter IC FAQs" by Timothy Hegarty, TI E2E™ design support forums, August 2023.

About The Author

Timothy Hegarty is a senior member of technical staff (SMTS) in the Switching Regulators business unit at Texas Instruments. With over 25 years of power management engineering experience, he has written numerous conference papers, articles, seminars, white papers, application notes and blogs. Tim's current focus is on enabling technologies for high-frequency, low-EMI, isolated and nonisolated regulators with wide input voltage range, targeting industrial, communications and automotive applications in particular. He is a senior member of the IEEE and a member of the IEEE Power Electronics, Industrial Applications and EMC Societies.

For more on EMI and EMC topics in power supply design, see the How2Power's Power Supply EMI Anthology.